



Influence of substrate temperature on the properties of ZnTe:Cu films prepared by a magnetron co-sputtering method

Hongwei Li^a, Haofei Huang^a, Azhati Lina^a, Ke Tang^{a,b,**}, Zhuorui Chen^a, Zilong Zhang^c, Ke Xu^a, Keke Ding^a, Linjun Wang^{a,b,d}, Jian Huang^{a,b,d,*}

^a School of Materials Science and Engineering, Shanghai University, Shanghai 200444, China

^b Zhejiang Institute of Advanced Materials, SHU, Jiashan 314113, China

^c Research Center for Functional Materials, National Institute for Materials Sciences (NIMS), Namiki 1-1, Tsukuba, Ibaraki 305-0044, Japan

^d Shanghai Collaborative Innovation Center of Intelligent Sensing Chip Technology, Shanghai, China

ARTICLE INFO

Keywords:

ZnTe:Cu film
Magnetron co-sputtering
Substrate temperature
Electrical properties

ABSTRACT

Copper-doped Zinc Tellurium (ZnTe:Cu) films were deposited on borosilicate glass using magnetron co-sputtering technique. The influence of the substrate temperature on the structural, morphological, optical and electrical properties of ZnTe:Cu films was investigated by X-ray diffraction (XRD), Raman spectroscopy, X-ray photoelectron spectroscopy (XPS), atomic force microscopy (AFM), UV–Vis spectrophotometer and Hall effect measurement system. The results indicate that substrate temperature significantly affects the properties of the ZnTe:Cu films. When the substrate temperature increases from room temperature to 600 °C, the (111)-preferred orientation of ZnTe:Cu films is gradually replaced by the (220)-preferred orientation. At high substrate temperatures (≥ 500 °C), the Cu_xTe phase appears in the ZnTe:Cu films, resulting in higher carrier concentration ($>10^{19} \text{ cm}^{-3}$) and lower resistivity ($<10^{-2} \Omega \text{ cm}$) of the prepared films.

1. Introduction

Zinc Tellurium (ZnTe) is a crucial semiconductor in the II-VI group with a wide bandgap. It has gained significant attention in recent years for its potential applications in optoelectronic devices due to its direct band gap of approximately 2.26 eV [1–4]. ZnTe, with its small valence-band offset (0.05 eV) to CdTe [5], is an excellent candidate material as a back contact for CdTe-based solar cells owing to its low resistivity. The ZnTe layer is usually deposited between the CdTe absorber and the metallization layer to realize a better ohmic contact. This triple-layer structure is in favor of the improvement of the fill factor and open-circuit voltage of the module [6]. Additionally, the similar structural characterization between ZnTe and CdZnTe (CZT) make it a suitable material to act as the back contact of CZT-based devices [7].

Generally speaking, high carrier concentration and low resistivity are required for back contact materials. To obtain the ZnTe films with high carrier concentration and low resistivity, p-type doping methods are commonly used. However, finding an appropriate p-type dopant for ZnTe films has been challenging. Various elements have been tried, including group V elements of N [8], P [9], As [10], Sb [11], Bi [12], and transition elements of Ag [13] and Cu [14]. Among these, the Cu doping is considered to be a cost-effective and

* Corresponding author. School of Materials Science and Engineering, Shanghai University, Shanghai 200444, China.

** Corresponding author. School of Materials Science and Engineering, Shanghai University, Shanghai 200444, China.

E-mail addresses: tangeke@shu.edu.cn (K. Tang), jianhuang@shu.edu.cn (J. Huang).

<https://doi.org/10.1016/j.heliyon.2023.e23349>

Received 5 June 2023; Received in revised form 30 November 2023; Accepted 1 December 2023

Available online 12 December 2023

2405-8440/© 2023 The Authors. Published by Elsevier Ltd. This is an open access article under the CC BY-NC-ND license (<http://creativecommons.org/licenses/by-nc-nd/4.0/>).

more efficient way of doping ZnTe films [15]. It is attributed that the Cu diffusion and Cu–Zn substitution process is easy to be achieved due to the alignment of ionic radius between Cu^{2+} and Zn^{2+} [16]. Therefore, Cu-doped ZnTe films typically exhibit higher carrier concentration ($>10^{18} \text{ cm}^{-3}$).

A variety of deposition techniques have been carried out to fabricate Cu doped ZnTe (ZnTe:Cu) films, including thermal evaporation [6,16,17], pulsed laser deposition (PLD) [18,19] and magnetron sputtering [20–22]. Among them, the magnetron sputtering process is simple and low cost, which is conducive to the deposition of ZnTe: Cu thin films with good adhesion and large area. However, since the magnetron sputtering system typically utilizes a mixed target of ZnTe: Cu with fixed composition, it restricts the ability to modify doping concentration. The magnetron co-sputtering technique, which employs two distinct targets (ZnTe and metallic Cu), was proposed to get around this problem.

In this work, ZnTe: Cu films were prepared using a magnetron co-sputtering technique. The effects of substrate temperature on the structure, morphology, optical and electrical properties of ZnTe: Cu films were studied in detail.

2. Experimental details

ZnTe:Cu films were deposited on ultrasonically cleaned borosilicate glass (2 cm \times 2 cm) using a magnetron co-sputtering technique at different substrate temperatures (room temperature, 100 °C, 200 °C, 300 °C, 400 °C, 500 °C and 600 °C). The co-sputtering process was executed by simultaneously operating a radio-frequency (RF) source (ZnTe target) and a direct current (DC) source (Cu target) in a vacuum chamber with a base pressure of 5×10^{-4} Pa. The growth parameters are as follows: Ar gas flow rate of 40 sccm, sputtering power of 100 W for the ZnTe target and 2 W for the Cu target. The ZnTe target and the metallic Cu target with high-purity ($>99.99\%$) were used during the deposition process. The total deposition time was set to 30 min, involving 10 min of pre-sputtering to avoid contamination. The substrate was rotated with a speed of 5 r/min to ensure film uniformity. The heating process was executed by a quartz lamp. The substrate temperature was confirmed through a thermocouple. In addition, undoped ZnTe films were produced under the same conditions to examine the impact of Cu doping on ZnTe:Cu film properties.

The film thickness was measured using a step profiler (Surfcorder ET150 from Kosaka Laboratory). The composition of the films was examined using an energy dispersive spectroscopy (EDS) device from Oxford Instruments. The structural and phase properties were investigated by using X-ray diffraction (XRD), Raman spectroscopy, and X-ray photoelectron spectroscopy (XPS). The XRD patterns were obtained by Rigaku Industrial Corporation D/MAX2200-3 kW, using $\text{Cu-K}\alpha_1$ radiation ($\lambda = 0.15406 \text{ nm}$) with a scan range between 20° and 80° and step length of 0.02° . The Raman spectra were measured by the HORIBA JOBIN YVON HR800 UV, with a 514 nm, 100 mW Ar^+ laser irradiation. The XPS spectra were obtained by Thermo ESCALAB 250Xi, using $\text{Al-K}\alpha$ radiation with a power of 150 W and beam spot size of 500 μm . The surface morphologies of the samples were observed via atomic force microscopy (AFM) with the tapping mode. The AFM examined area is $3 \mu\text{m} \times 3 \mu\text{m}$. The UV–Vis spectrophotometer was used to investigate the optical properties of samples with a wavelength range of 400–1000 nm, a bandwidth of 1 nm and a step of 0.5 nm. The electrical properties of the samples were characterized by a Hall effect measurement system (Accent model HL5500PC).

3. Results and discussion

3.1. Structural properties

The XRD patterns of ZnTe:Cu films in Fig. 1 reveal that ZnTe:Cu films exhibit two distinct diffraction peaks at approximately 25.4°

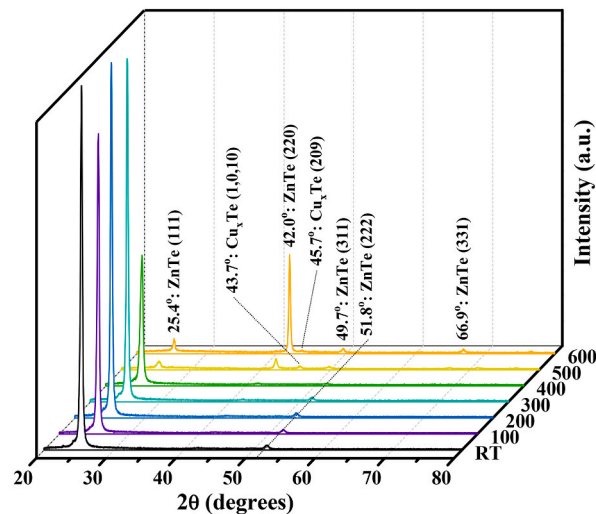


Fig. 1. XRD patterns of ZnTe:Cu films deposited under different substrate temperatures.

and 51.8° when the substrate temperature is below 400°C , which correspond to the (111) and (222) planes of cubic ZnTe (c-ZnTe) phase (JCPDS card No. 75-2085), respectively. The second-order diffraction of the (111) crystal plane produces a diffraction peak of (222). During the growth of the polycrystalline ZnTe films, this preferred orientation above commonly appears due to the low crystallization energy for forming (111)-oriented plane. A new diffraction peak corresponding to (220)-oriented c-ZnTe emerges at around 42.0° as the substrate temperature exceeds 400°C , and its intensity increases with higher temperatures. Additionally, the (111) diffraction peak gradually disappears while two weak diffraction peaks at 49.7° and 66.9° emerge, corresponding to the (311) and (331) peaks of c-ZnTe, respectively. Two other peaks at about 43.7° and 45.7° cannot be matched to the phase structure of c-ZnTe. To clarify the origins of these peaks, the XRD characterization of undoped ZnTe films was performed (Fig. 2).

In general, during the growth process of the ZnTe:Cu film, secondary phases and clusters of hexagonal ZnTe (h-ZnTe) or Cu_xTe may appear at elevated substrate temperatures or under post-annealing treatment [18,21,23]. Fig. 2 (a) and (b) indicate no significant difference between the doped and undoped samples deposited at room temperature (RT) and 300°C . When the substrate temperature is raised to 500°C , a new diffraction peak appears at 45.7° in the doped sample compared to the undoped sample (Fig. 2(C)), corresponding to the Cu_xTe phase (JCPDS card No. 45-1283). Compared to undoped ZnTe, the diffraction peak intensity of the (220) crystal plane of Cu-doped ZnTe films remains basically unchanged, while the peak intensity of the (111) crystal plane significantly decreases. This suggests that at higher substrate temperatures ($\geq 500^\circ\text{C}$), the formation of Cu_xTe disrupts some crystal structures, leading to a weakening of the preferred orientation of the (111) crystal plane. In addition, for undoped samples, as the substrate temperature increases, the preferred orientation of the (111) crystal plane exists, while the diffraction peak intensity of the (220) crystal plane continuously increases. This indicates that a higher substrate temperature provides greater crystallization energy, leading to the formation of preferred orientation of crystal planes with higher crystallization energy, such as (220) and (311).

Fig. 3 shows the Raman spectra of ZnTe:Cu films prepared under different substrate temperatures. The strongest peak, located at

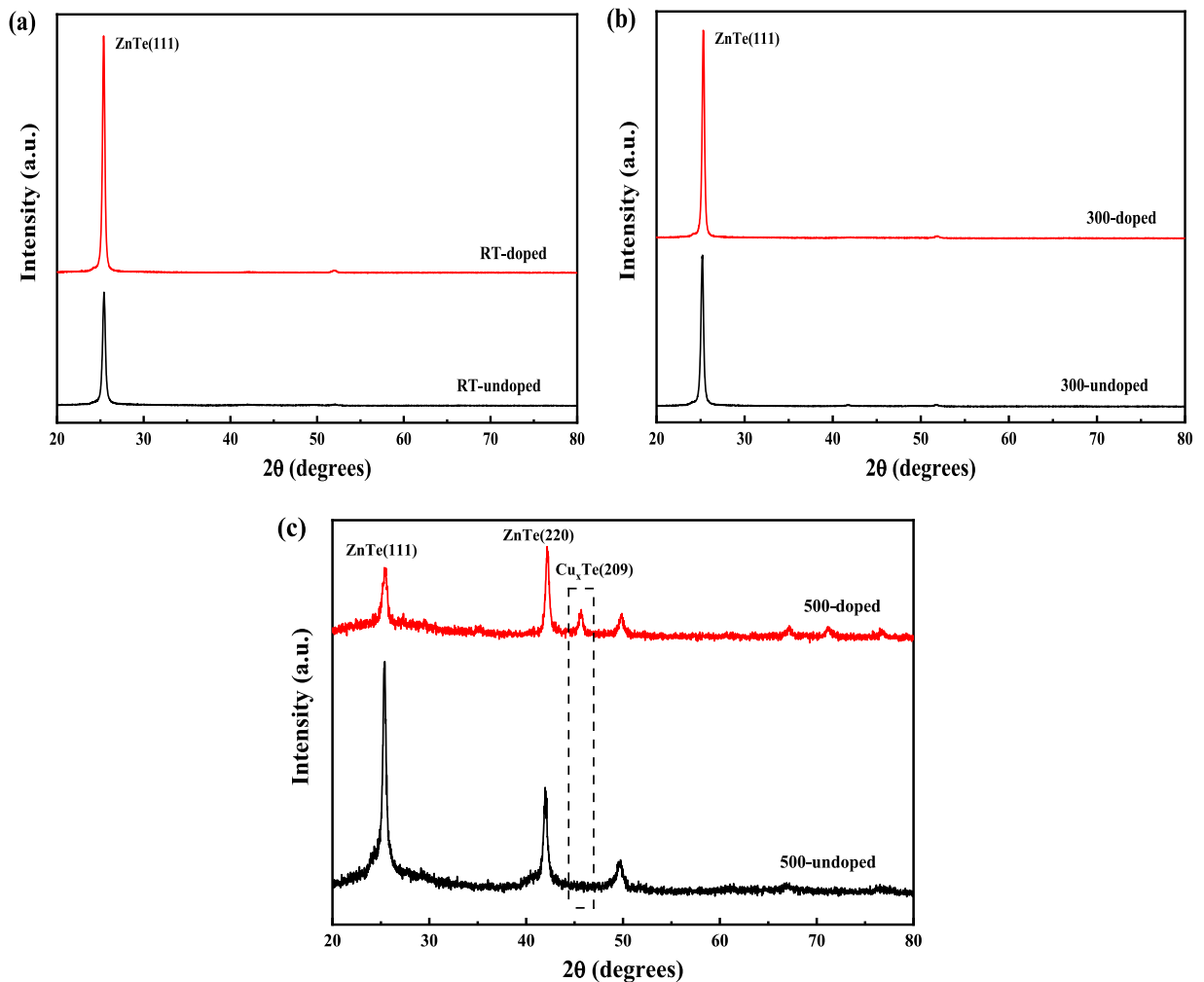


Fig. 2. XRD patterns of undoped and Cu-doped ZnTe films grown under different substrate temperatures: (a) RT; (b) 300°C ; (c) 500°C .

207 cm^{-1} , corresponds to the ZnTe LO mode [24]. Additionally, a peak at around 179 cm^{-1} indicates the presence of the ZnTe TO mode in the spectra of samples deposited at substrate temperatures of 500 °C and 600 °C. In the spectra of other samples, a "rise" centered from 164 cm^{-1} to 173 cm^{-1} is observed, with the centers of the "rises" encountering different levels of redshift. Similar redshifts of the TO peak at about 165 cm^{-1} have been reported [25]. The reduction in substrate temperature results in a greater redshift of the peak, which is attributed to the internal stress induced by the lattice mismatch between film and substrate. The other two peaks at about 410 cm^{-1} and 616 cm^{-1} of the Raman spectra, correspond to the second and third order of ZnTe LO mode, respectively. These findings are supported by previous research [26].

In addition, although Te phonon modes (the most common examples being the A1 mode at 122 cm^{-1} and the E2 mode at 142 cm^{-1}) have been reported in other works of undoped ZnTe films [27–29], no similar results were found in this study. This may be because for Cu doped ZnTe films, excess Te is prone to combine with Cu to form Cu_xTe , which is consistent with the results of XRD.

3.1.1. X-ray photoelectron spectroscopy

To investigate the chemical bonding characteristics of the Te, Zn, and Cu elements in co-sputtered ZnTe:Cu films, XPS survey was conducted. Fig. 4 shows the original and Voigt-fitted Te3d, Zn2p, and Cu2p XPS core level spectra of samples deposited at RT, 300 °C, and 500 °C. Distinctive changes in these spectra take place in samples deposited at 500 °C for all three elements. The intensity of peaks increases and all the peaks have a shift of 1.2 eV towards lower binding energy. This increase can be explained by morphology change, which is also observed in Raman spectra analysis, as both techniques are morphology sensitive. However, chemical environment may also be involved [30]. Test errors were ruled out because the locations of the C1s peaks (not plotted) of all samples align well.

In Fig. 4(a), four peaks of Te3d are observed, consisting of two Te3d_{3/2} and Te3d_{5/2} doublet peaks of Te and oxide Te. The doublet peaks of Te indicate the presence of ZnTe, and previous testing showed no sign of a pure Te phase. For RT and 300 °C samples, the intensity of Te peaks is almost as strong as that of oxide Te peaks. It was previously hypothesized that Cu catalyzed the oxidation of tellurium, which could explain this observation [5]. However, this hypothesis is not sufficient to account for the increased intensity of oxide Te peaks for samples taken at 500 °C, which is considerably stronger than that of Te peaks. Another study discovered that the Cu_xTe -related Te3d peaks are in nearly the same location as TeO_2 -related peaks [31], which suggests that at 500 °C, the oxide Te peaks are the result of both Te oxidation and Cu_xTe .

There are two separated peaks for all Zn2p and Cu2p spectra in Fig. 4 (b) and (c) represents the 2p_{1/2} and 2p_{3/2} doublet peaks of Zn and Cu. The peaks of Zn2p are typical of the Zn–Te bond. The chemical state of Cu cannot be recognized specifically by the peaks of Cu2p though, since the binding energies for Cu^0 , Cu^{1+} and Cu^{2+} are all close to 0.05 eV [32].

3.2. Surface morphology

The atomic force microscopy (AFM) was utilized to obtain the topography characteristics of ZnTe:Cu films. Fig. 5 displays the 3D micrographs with topographical features of representative samples with substrate temperatures of RT, 300 °C, and 500 °C. The root-mean-square (RMS) roughness was calculated and was presented in the corresponding figure. For the RT sample in Fig. 5 (a), the grain size is relatively small. In Fig. 5 (b), the surface morphology of the 300 °C samples is similar to that of the RT sample, except that a small number of larger grains appear in the 300 °C samples. The RMS roughness of the 300 °C samples rises from 1.44 nm to 1.97 nm. Fig. 5 (c) indicates that the RMS roughness of the 500 °C samples increased to 11.59 nm. This is attributed to recrystallization occurring in the film as the substrate temperature increased.

In addition, the step profiler is also a device used to characterize surface morphology and characteristics, and can accurately measure the average thickness of thin films. An accurate step meter was used to measure the thickness of thin films grown at different substrate temperatures, and the growth rate of the thin films was further determined based on the growth time. From Table 1, it can be

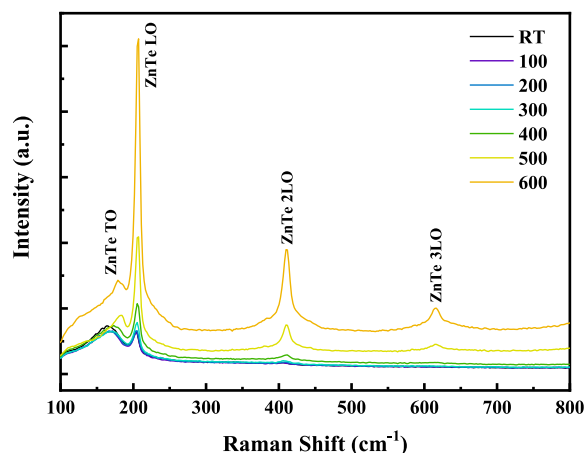


Fig. 3. Raman spectra of ZnTe:Cu films deposited under different substrate temperatures.

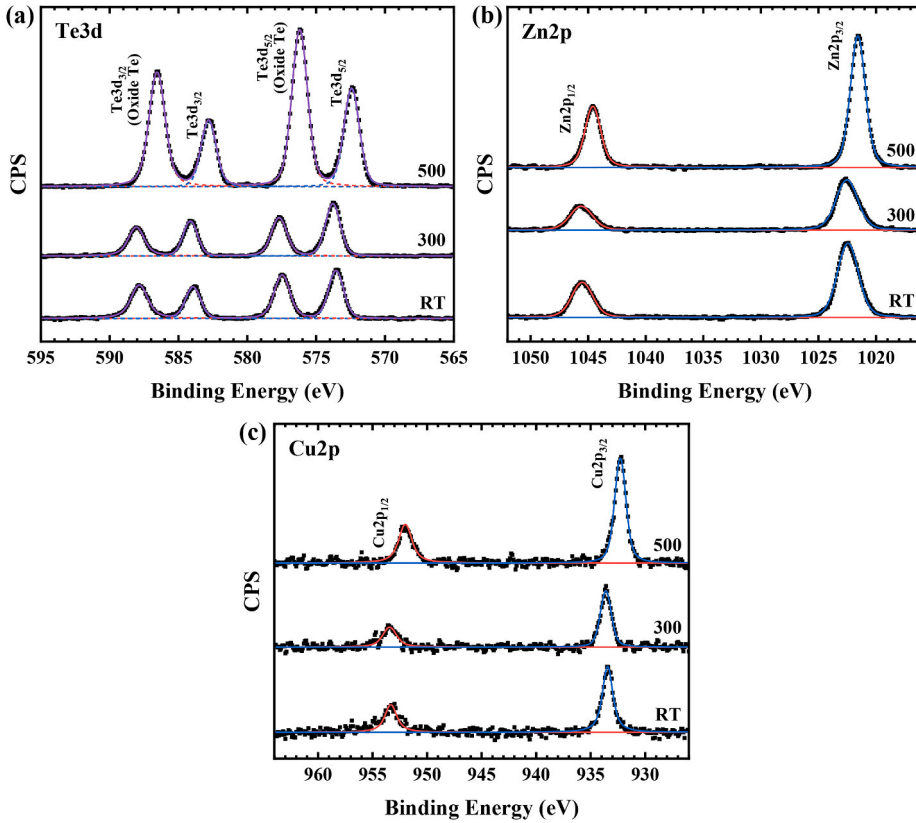


Fig. 4. XPS core level spectra of ZnTe:Cu films deposited at RT, 300 °C and 500 °C: (a) Te3d (solid line for cumulative fitted curve and dashed line for each peak fitted); (b) Zn2p; (c) Cu2p.

concluded that the thickness of all samples is around 600 nm, as the substrate temperature increases, the growth rate of the thin film gradually accelerates.

3.3. Optical properties

The transmittance spectra and band gap values were analyzed to investigate the optical properties of ZnTe:Cu films deposited at various substrate temperatures. Fig. 6 (a) depicts the acquired transmittance spectra of samples in the 400–1000 nm range at all substrate temperatures. The results indicate that within the visible light range, the transmittance of ZnTe:Cu films slightly increases with the increase of substrate temperature.

For direct band gap materials, optical band gap energy (E_g) can be determined using Tauc’s direct optical transition model [33], given as follows:

$$\alpha h\nu = A(h\nu - E_g)^{1/2} \tag{1}$$

where α is the absorption coefficient, $h\nu$ is photon energy, and A is a constant depending on the optical transition probability. Through equation (1), it can be known that there is a linear relationship between $(\alpha h\nu)^2$ and $h\nu$, which can be used to calculate the value of E_g . The absorption coefficient α can be calculated with transmittance data by equation (2) as shown in the following relationship:

$$\alpha = \frac{1}{d} \ln\left(\frac{1}{T}\right) \tag{2}$$

where d is the film thickness and T is the transmittance. Fig. 6 (b) shows the Tauc plot of the samples, where $(\alpha h\nu)^2$ is plotted as a function of $h\nu$. By extrapolating the linear parts of the curves, intercept values on the x-axis ($h\nu$) can be obtained, which correspond to the values of E_g . The E_g of all samples is lower than that of crystalline ZnTe (2.26 eV), which is due to the band gap narrowing effect caused by Cu doping, which is common when the semiconductor material is heavily doped [34].

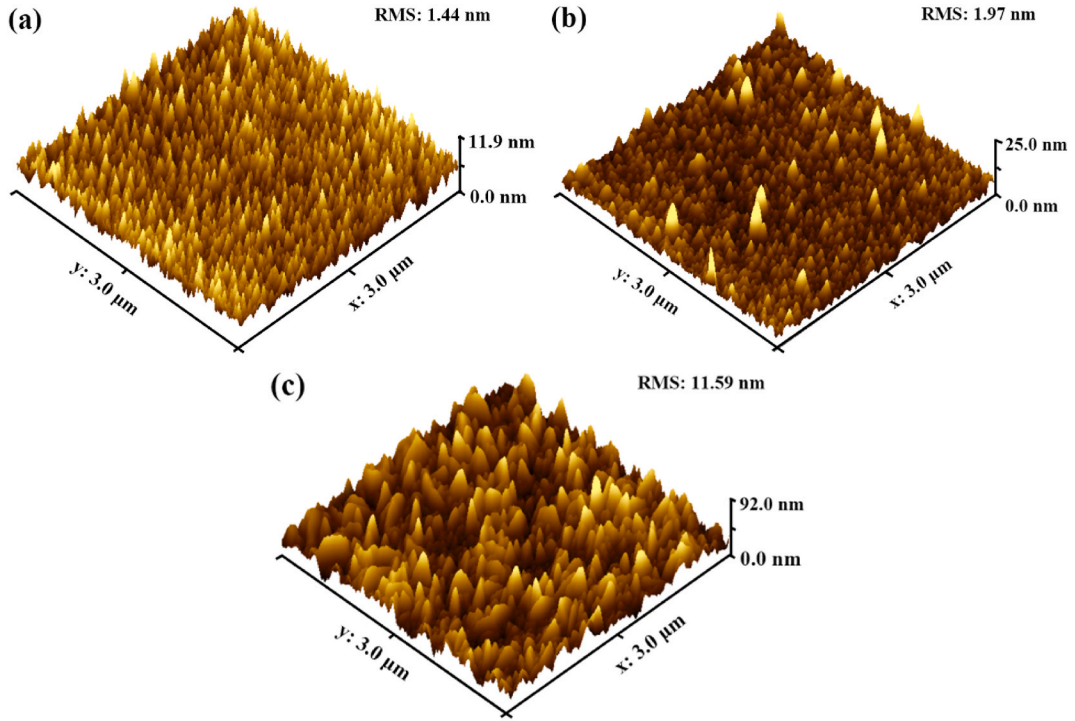


Fig. 5. AFM images of ZnTe:Cu films deposited at: (a) RT; (b) 300 °C; (c) 500 °C.

Table 1

Analysis of the film thickness results of the step profiler test.

Substrate temperature	film thickness	deposition time	growth rate
RT	568.4 nm	1200s	0.4737 nm/s
100 °C	593.5 nm		0.4946 nm/s
200 °C	575.4 nm		0.4795 nm/s
300 °C	598.8 nm		0.4990 nm/s
400 °C	595.6 nm		0.4963 nm/s
500 °C	604.6 nm		0.5308 nm/s
600 °C	642.8 nm		0.5375 nm/s

3.4. Electrical properties

The semiconductor Hall effect tester is widely used to measure important parameters such as carrier concentration, mobility, resistivity, Hall coefficient, carrier type, block resistance, etc. of semiconductor materials. It can be used for films or bulk materials, and its principle is mainly based on the van der Pauw method. This method does not have special requirements for the shape of the sample, but requires a uniform thickness of the thin film sample and no holes on the surface. All ZnTe:Cu films are dense and uniform in thickness with a surface size of 2 cm × 2 cm. Electrodes were grown at the four corners of the film sample edges for Hall testing. Table 2 shows Hall effect measurements results of ZnTe:Cu films deposited at different temperature, and Fig. 7 visualizes the carrier concentration, Hall mobility, and resistivity changing trend with increasing substrate temperature. To expound on the findings, we introduce the grain boundary trapping theory developed by Seto [35], which is based on three assumptions: (1) the polycrystalline film is composed of identical crystallites with a grain size of L cm; (2) there is only one type of impurity atom present, the impurity atoms are totally ionized and are uniformly distributed with a concentration of N/cm^3 ; (3) the grain boundary is of negligible thickness compared to L and contains Q_t/cm^2 traps located at specific energy with respect to the intrinsic Fermi level. The grain boundary energy barrier E_B can then be given as follows:

$$E_B = \frac{q^2 L^2 N}{8\epsilon} \quad (LN < Q_t) \quad (3)$$

$$E_B = \frac{q^2 Q_t^2}{8\epsilon N} \quad (LN > Q_t) \quad (4)$$

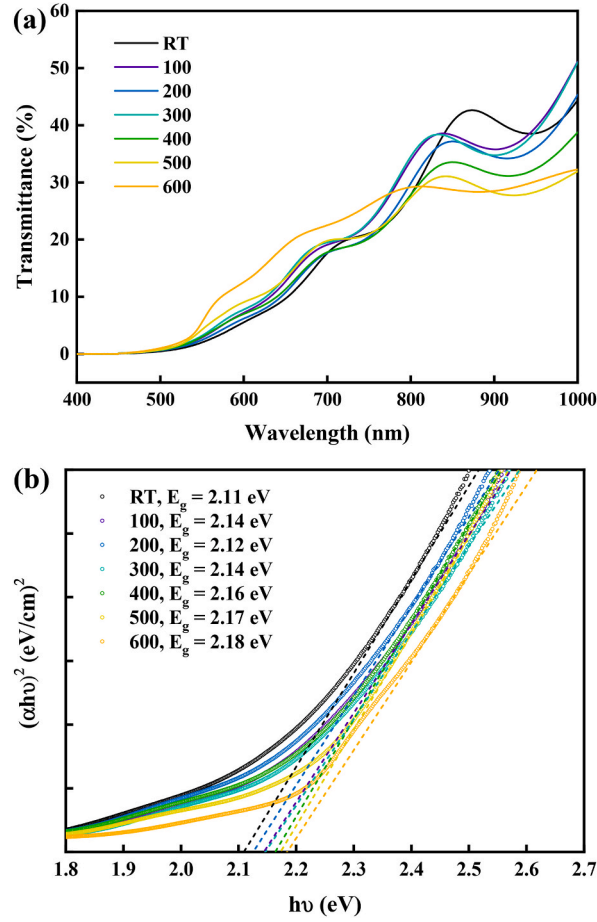


Fig. 6. (a) Transmittance spectra and (b) Tauc plot of ZnTe:Cu films deposited at different substrate temperatures.

Table 2

Hall effect measurements of ZnTe:Cu films deposited at different temperatures.

Substrate temperature (°C)	Carrier concentration (cm ⁻³)	Hall mobility (cm ² V ⁻¹ s ⁻¹)	Resistivity (Ω-cm)
RT	4.866 × 10 ¹⁷	3.410	3.760
100	4.881 × 10 ¹⁸	2.230	0.574
200	4.729 × 10 ¹⁸	2.140	0.615
300	1.846 × 10 ¹⁸	2.490	1.360
400	1.076 × 10 ¹⁸	3.340	1.735
500	1.177 × 10 ¹⁹	12.100	0.044
600	1.071 × 10 ¹⁹	11.200	0.052

where q is the quantity of electric charge and ε is the dielectric permittivity. When $LN < Q_b$, the additional carriers brought by increasing the number of effective dopants will compensate for the traps first, thus causing E_B to rise. The increased dopants can truly begin to lower the barrier only when $LN > Q_t$. Moreover, the following relationship exists between the mobility μ and the resistivity ρ of the polycrystalline film:

$$\mu \propto \exp\left(-\frac{E_B}{kT}\right) \quad (5)$$

$$\rho = \frac{1}{q\rho\mu} \quad (6)$$

where p is the average carrier concentration of the film.

The carrier concentration of ZnTe:Cu polycrystalline films deposited at different substrate temperatures varies. The carrier

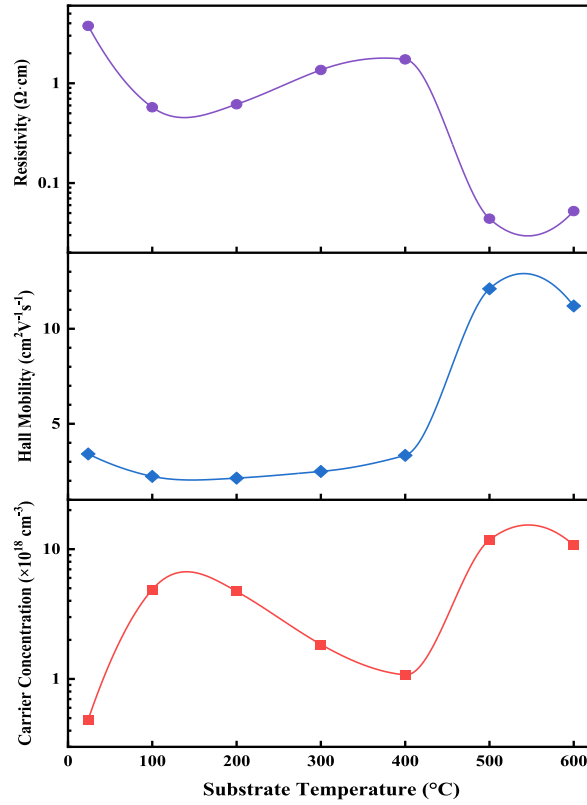


Fig. 7. The carrier concentration, Hall mobility and resistivity of the ZnTe:Cu films as a function of substrate temperature.

concentration of the RT sample is the lowest, within 10^{17} cm^{-3} . Cu atoms tend to stay at grain boundaries when deposited at room temperature with the co-evaporation technique [36]. A similar process may happen during co-sputtering process in this work, where the major part of the sputtered Cu atoms doesn't participate in the ZnTe nucleation and growth process, only settling at the grain boundaries. Since these Cu atoms are in the form of Cu^0 , they are unable to provide additional carriers to the film, making themselves invalid dopants.

When the substrate temperature rises to the range of 100 °C and 200 °C, the carrier concentration sharply increases by an order of magnitude, indicating that some of the Cu atoms at the grain boundaries are thermally ionized, becoming Cu^{1+} or Cu^{2+} , and are able to diffuse into the ZnTe lattice to become effective dopants. This results in an increase of N . However, LN is still lower than Q_b , so equation (3) should still be adopted, and therefore E_B should increase linearly and μ should accordingly drop down. When the substrate temperature reaches 300 °C, the carrier concentration does not continue to increase but begins to decline due to the further ionization of Cu^{1+} to Cu^{2+} , leading to its loss of effect as an acceptor impurity. As N decreases, μ increases slightly. The same illustration could also be applied to the 400 °C sample.

Notably, a significant variation occurs in the samples when the substrate temperature is raised to 500 °C and 600 °C, mainly reflected in structure alterations, increased grain size, and formation of the Cu_xTe phase. The formation of the Cu_xTe phase can not only provide additional free carriers and increase the carrier concentration of the film, but also passivate the defects in grain boundaries. Combined with grain boundary trapping theory, these changes correspond to the increase of L and N and the decrease of Q_b , respectively. Equation (4) is applicable when $LN > Q_b$, and the correlation between E_B and N changes from positive to negative. Combination with equation (5), μ will increase as N increases. Since the carrier concentration and mobility are increasing at this time, ρ is greatly reduced according to equation (6). The variation of electrical properties of ZnTe: Cu thin films with substrate temperature can be well explained by the grain boundary trapping theory.

The ZnTe:Cu films acquire both high carrier concentration ($>10^{19} \text{ cm}^{-3}$) and low resistivity ($<10^{-2} \Omega \text{ cm}$) at a high substrate temperature (500 °C or higher), representing their appealing electrical performances and their great potential in corresponding applications.

4. Conclusions

This work meticulously examines how substrate temperature affects the properties of ZnTe:Cu films deposited on borosilicate glass by magnetron co-sputtering using two individual targets. The films displayed excellent surface flatness and uniformity across all substrate temperatures. At lower substrate temperatures ($\leq 400 \text{ °C}$), the films exhibited a (111)-preferred orientation. However, as the

substrate temperature increases (≥ 500 °C), the original (111) preferred orientation of ZnTe: Cu films weakens, while the (220) preferred orientation gradually increases. At this stage, the formation of Cu_xTe compounds in the ZnTe:Cu film significantly improved its electrical properties, with carrier concentrations exceeding 10^{19} cm^{-3} and resistivity within $10^{-2} \Omega \text{ cm}$. The variation in the electrical properties of the ZnTe:Cu films with substrate temperature was consistent with the grain boundary trapping theory. These high-performance ZnTe:Cu films, prepared by magnetron co-sputtering, show great potential for device applications.

Data availability statement

All data included in this study are available upon request by contact with the corresponding author.

CRediT authorship contribution statement

Hongwei Li: Writing - review & editing, Writing - original draft, Investigation, Data curation, Conceptualization. **Haofei Huang:** Writing - review & editing, Writing - original draft, Formal analysis. **Azhati Lina:** Writing - original draft, Investigation. **Ke Tang:** Writing - review & editing, Resources. **Zhuorui Chen:** Investigation, Formal analysis. **Zilong Zhang:** Writing - review & editing, Resources, Investigation. **Ke Xu:** Investigation. **Keke Ding:** Investigation. **Linjun Wang:** Resources. **Jian Huang:** Writing - review & editing, Resources, Formal analysis.

Declaration of competing interest

The authors declare that they have no known competing financial interests or personal relationships that could have appeared to influence the work reported in this paper.

Acknowledgments

This work was funded by the National Natural Science Foundation of China (No.11875186, No.11905121).

References

- [1] K.S. Lee, G. Oh, E.K. Kim, High performance intermediate-band solar cells based on ZnTe:Cr with ZnO:Al electron transport layer, *Sol. Energy* 164 (2018) 262–266, <https://doi.org/10.1016/j.solener.2018.02.074>.
- [2] X.W. Ju, D.R. Chen, X.C. Chen, T. Gao, Y. Chen, J. Wang, X.F. Wang, Significant enhancement of THz detectivity by lowering ZnTe crystal temperature in electro-optic sampling, *Opt. Mater.* 91 (2019) 235–238, <https://doi.org/10.1016/j.optmat.2019.03.021>.
- [3] P. Baranowski, M. Szymura, G. Karczewski, M. Aleszkiewicz, A. Rodek, T. Kazimierzczuk, P. Kossacki, T. Wojtowicz, J. Kossut, P. Wojnar, Optical signatures of type I-type II band alignment transition in Cd(Se,Te)/ZnTe self-assembled quantum dots, *Appl. Phys. Lett.* 117 (2020), 113101, <https://doi.org/10.1063/5.0016326>.
- [4] T.A. Gessert, A.R. Mason, P. Sheldon, A.B. Swartzlander, D. Niles, T.J. Coutts, Development of Cu-doped ZnTe as a back-contact interface layer for thin-film CdS/CdTe solar cells, *J. Vac. Sci. Technol. A* 14 (1996) 806–812, <https://doi.org/10.1116/1.580394>.
- [5] W.W. Wang, G.P. Xia, J.G. Zheng, L.H. Feng, R.Y. Hao, Study of polycrystalline ZnTe (ZnTe:Cu) films for photovoltaic cells, *J. Mater. Sci. Mater. Electron.* 18 (2007) 427–431, <https://doi.org/10.1007/s10854-006-9044-0>.
- [6] C.A. Wolden, A. Abbas, J.J. Li, D.R. Diercks, D.M. Meysing, T.R. Ohno, J.D. Beach, T.M. Barnes, J.M. Walls, The roles of ZnTe buffer layers on CdTe solar cell performance, *Sol. Energy Mater. Sol. Cells* 147 (2016) 203–210, <https://doi.org/10.1016/j.solmat.2015.12.019>.
- [7] K.F. Qin, H.H. Ji, J. Huang, K. Tang, Y.B. Shen, X.T. Zhang, M. Cao, J.J. Zhang, Y. Shen, L.J. Wang, The effects of Cu-doped ZnTe intermediate layer on the Ohmic contact to CdZnTe films, *Surf. Coat. Technol.* 320 (2017) 366–370, <https://doi.org/10.1016/j.surfcoat.2016.12.027>.
- [8] K.S. Lee, G. Oh, E.K. Kim, Growth of p-type ZnTe films by using nitrogen doping during pulsed laser deposition, *J. Kor. Phys. Soc.* 67 (2015) 672–675, <https://doi.org/10.3938/jkps.67.672>.
- [9] M. Nishio, K. Saito, Y. Nakatsuru, T. Shono, Y. Matsuo, A. Tomota, T. Tanaka, Q.X. Guo, Photoluminescence and electrical properties of P-doped ZnTe layers grown by low pressure MOVPE, *J. Cryst. Growth* 468 (2017) 666–670, <https://doi.org/10.1016/j.jcrysgro.2017.01.030>.
- [10] O. Oklobia, G. Kartopu, S.J.C. Irvine, Properties of arsenic-doped ZnTe films as a back contact for CdTe solar cells, *Materials* 12 (2019) 3706, <https://doi.org/10.3390/ma12223706>.
- [11] A. Barati, A. Klein, W. Jaegermann, Deposition and characterization of highly p-type antimony doped ZnTe films, *Thin Solid Films* 517 (2009) 2149–2152, <https://doi.org/10.1016/j.tsf.2008.10.078>.
- [12] G.K. Rao, G.K. Shivakumar, V.B. Kasturi, The p-type doping of vacuum deposited ZnTe films with bismuth by a new technique of using nano-spheres, *Mater. Sci. Eng. B-Adv. Funct. Solid-State Mater.* 175 (2010) 185–188, <https://doi.org/10.1016/j.mseb.2010.07.012>.
- [13] A.K.S. Aqili, A. Maqsood, Z. Ali, Properties of Ag doped ZnTe films by an ion exchange process, *Appl. Surf. Sci.* 191 (2002) 280–285, [https://doi.org/10.1016/S0169-4332\(02\)00218-0](https://doi.org/10.1016/S0169-4332(02)00218-0).
- [14] A.K.S. Aqili, A. Maqsood, Z. Ali, Properties of copper-doped ZnTe films by immersion in Cu solution, *Appl. Surf. Sci.* 180 (2001) 73–80, [https://doi.org/10.1016/S0169-4332\(01\)00315-4](https://doi.org/10.1016/S0169-4332(01)00315-4).
- [15] J.J. Li, D.R. Diercks, T.R. Ohno, C.W. Warren, M.C. Lonergan, J.D. Beach, C.A. Wolden, Controlled activation of ZnTe:Cu contacted CdTe solar cells using rapid thermal processing, *Sol. Energy Mater. Sol. Cells* 133 (2015) 208–215, <https://doi.org/10.1016/j.solmat.2014.10.045>.
- [16] Q. Gul, M. Zakria, T.M. Khan, A. Mahmood, A. Iqbal, Effects of Cu incorporation on physical properties of ZnTe films deposited by thermal evaporation, *Mater. Sci. Semicond. Process.* 19 (2014) 17–23, <https://doi.org/10.1016/j.mssp.2013.11.033>.
- [17] B.C. Chen, J.H. Liu, Z.X. Cai, A. Xu, X.L. Liu, Z.T. Rong, D.H. Qin, W. Xu, L.T. Hou, Q.B. Liang, The effects of ZnTe:Cu back contact on the performance of CdTe nanocrystal solar cells with inverted structure, *Nanomaterials* 9 (2019) 626, <https://doi.org/10.3390/nano9040626>.
- [18] G. Lastra, P.A. Luque, M.A. Quevedo-Lopez, A. Olivas, Electrical properties of p-type ZnTe films by immersion in Cu solution, *Mater. Lett.* 126 (2014) 271–273, <https://doi.org/10.1016/j.matlet.2014.04.058>.
- [19] F.J. Ochoa-Estrella, A. Vera-Marquina, I. Mejia, A.L. Leal-Cruz, M.I. Pintor-Monroy, M. Quevedo-Lopez, Structural, optical, and electrical properties of ZnTe:Cu films by PLD, *J. Mater. Sci. Mater. Electron.* 29 (2018) 20623–20628, <https://doi.org/10.1007/s10854-018-0200-0>.
- [20] A. Bosio, R. Ciprian, A. Lamperti, I. Rago, B. Ressel, G. Rosa, M. Stupar, E. Weschke, Interface phenomena between CdTe and ZnTe:Cu back contact, *Sol. Energy* 176 (2018) 186–193, <https://doi.org/10.1016/j.solener.2018.10.035>.

- [21] S. Ulicna, P.J.M. Isherwood, P.M. Kaminski, J.M. Walls, J. Li, C.A. Wolden, Development of ZnTe as a back contact material for thin film cadmium telluride solar cells, *Vacuum* 139 (2017) 159–163, <https://doi.org/10.1016/j.vacuum.2017.01.001>.
- [22] F. El Akkad, M. Mathai, Structural and luminescence properties of heavily doped radio-frequency-sputtered ZnTe:Cu films, *J. Appl. Phys.* 118 (2015), 095706, <https://doi.org/10.1063/1.4929876>.
- [23] B.R. Faulkner, T.R. Ohno, J.M. Burst, J.N. Duenow, C.L. Perkins, B. To, T.A. Gessert, The effects of sputtering target preparation and deposition temperature on ZnTe:Cu film properties, in: 2015 Ieee 42nd Photovoltaic Specialist Conference, Ieee, New York, 2015. <https://ieeexplore.ieee.org/document/7356097>.
- [24] J.C. Irwin, J. Lacombe, Raman scattering in ZnTe, *J. Appl. Phys.* 41 (1970) 1444–1450, <https://doi.org/10.1063/1.1659054>.
- [25] O.I. Olusola, M.L. Madugu, N.A. Abdul-Manaf, I.M. Dharmadasa, Growth and characterisation of n- and p-type ZnTe films for applications in electronic devices, *Curr. Appl. Phys.* 16 (2016) 120–130, <https://doi.org/10.1016/j.cap.2015.11.008>.
- [26] H. Singh, M. Singh, J. Singh, B.S. Bansod, T. Singh, A. Thakur, M.F. Wani, J. Sharma, Composition dependence study of thermally evaporated nanocrystalline ZnTe films, *J. Mater. Sci. Mater. Electron.* 30 (2019) 3504–3510, <https://doi.org/10.1007/s10854-018-00627-9>.
- [27] Y. Du, G. Qiu, Y. Wang, M. Si, X. Xu, W. Wu, P.D. Ye, One-dimensional van der Waals material tellurium: Raman spectroscopy under strain and magneto-transport, *Nano Lett.* 17 (2017) 3965–3973, <https://doi.org/10.1021/acs.nanolett.7b01717>.
- [28] L.N. Zhang, C. Liu, Q.M. Yang, L.J. Cui, Y.P. Zeng, Growth and characterization of highly nitrogen doped ZnTe films on GaAs (001) by molecular beam epitaxy, *Mater. Sci. Semicond. Process.* 29 (2015) 351–356, <https://doi.org/10.1016/j.mssp.2014.06.045>.
- [29] F.J. Ochoa-Estrella, A. Vera-Marquina, I. Mejia, A.L. Leal-Cruz, M. Quevedo-Lopez, Pressure influence on structural and optical behaviors of ZnTe films grown by PLD, *J. Mater. Sci. Mater. Electron.* 29 (2018) 7629–7636, <https://doi.org/10.1007/s10854-018-8755-3>.
- [30] T. Potlog, D. Duca, M. Dobromir, Temperature-dependent growth and XPS of Ag-doped ZnTe films deposited by close space sublimation method, *Appl. Surf. Sci.* 352 (2015) 33–37, <https://doi.org/10.1016/j.apsusc.2015.03.133>.
- [31] F. El Akkad, Y. Abdulraheem, Morphology, electrical, and optical properties of heavily doped ZnTe:Cu films, *J. Appl. Phys.* 114 (2013), 183501, <https://doi.org/10.1063/1.4829453>.
- [32] G. Teeter, X-ray and ultraviolet photoelectron spectroscopy measurements of Cu-doped CdTe(111)-B: observation of temperature-reversible Cu_xTe precipitation and effect on ionization potential, *J. Appl. Phys.* 102 (2007), 034504, <https://doi.org/10.1063/1.2759876>.
- [33] H.H. Gullu, O.B. Surucu, M. Isik, M. Terlemozglu, M. Parlak, Material and Si-based diode analyses of sputtered ZnTe films, *J. Mater. Sci. Mater. Electron.* 31 (2020) 11390–11397, <https://doi.org/10.1007/s10854-020-03688-x>.
- [34] K.F. Berggren, B.E. Sernelius, Band-gap narrowing in heavily doped many-valley semiconductors, *Phys. Rev. B* 24 (1981) 1971–1986, <https://doi.org/10.1103/PhysRevB.24.1971>.
- [35] J.Y.W. Seto, The electrical properties of polycrystalline silicon, *J. Appl. Phys.* 46 (1975) 5247–5254, <https://doi.org/10.1063/1.321593>.
- [36] J.Q. Zhang, L.H. Feng, W. Cai, J.G. Zheng, Y.P. Cai, B. Li, L.L. Wu, Y. Shao, The structural phase transition and mechanism of abnormal temperature dependence of conductivity in ZnTe:Cu polycrystalline films, *Thin Solid Films* 414 (2002) 113–118, [https://doi.org/10.1016/S0040-6090\(02\)00451-0](https://doi.org/10.1016/S0040-6090(02)00451-0).